Journal of Catalysis **186,** 433–441 (1999)
Article ID jcat.1999.2557, available online at http://www.idealibrary.com on IDEAL®

Sintering of Chlorinated Pt/γ-Al_2O_3 Catalysts: An *In Situ* Study by X-Ray Absorption Spectroscopy

A. Borgna,*[,1] T. F. Garetto,* C. R. Apesteguía,* F. Le Normand,†[,2] and B. Moraweck‡

*INCAPE (UNL-CONICET), Santiago del Estero 2654, (3000) Santa Fe, Argentina; †LERSCI, Université Louis Pasteur, 4 Rue Blaise Pascal, F 67070 Strasbourg, France; and ‡Institut de Recherches sur la Catalyse, CNRS, 2 Avenue Albert Einstein, F 69626 Villeurbanne, France

Received March 24, 1998; revised December 11, 1998; accepted May 13, 1999

In situ **EXAFS spectroscopy was used for identifying the surface species involved in the sintering of alumina-supported Pt catalysts under dried oxidizing atmospheres. A Pt/γ-Al_2O_3 catalyst (0.62 wt% Pt, 0.88 wt% Cl) was heated in a 2% O_2/N_2 gaseous mixture from 300 to 525°C for about 120 min and then kept at this temperature for up to 720 min. The main observation, which is in good agreement with** *ex situ* **TPR experiments, was that chlorine is always present in the surrounding of platinum during the oxidizing treatment. The metal sintering process involved three successive steps during which the chlorine and oxygen coordinations passed through a maximum, whereas platinum coordination exhibited a minimum. Formation of $Pt(OH)_4Cl_2$ species was detected at the end of the first step, i.e., when the temperature reached 500°C. After about 4 h of treatment, we deduced that platinum species are made up of a metal platinum core surrounded by a double coating of oxychlorinated species. More precisely, EXAFS experiments suggested that surface platinum oxide is made of rigid PtO_6 octahedra, but their assembly led to a largely disordered structure. The absence of a long-range order allows the location of residual chlorine species either between the PtO_6 octahedra or at the Pt-oxidized surface shell.**

Key Words: **sintering; EXAFS; reforming catalysts; chlorine; oxychlorinated species; "cherry" model.**

1. INTRODUCTION

Under industrial conditions, sintering of Pt-based naphtha reforming catalysts occurs mainly during the *in situ* catalyst regeneration, which is performed under oxidizing atmospheres. When coke burning is carried out, both the high exothermicity of the reaction and the formation of water cause the platinum crystallites to grow. The low oxygen pressure used to avoid a dangerous increase in the reactor temperature favors the sintering of the metallic fraction (1). To prevent platinum particle growth, chlorided compounds are usually added to the oxidizing mixture (2). The chemical nature of surface intermediate species plays a key role in determining the kinetics of platinum sintering (3). However, very few studies have employed *in situ* characterization techniques, which are required to follow the formation kinetics of intermediate oxy- or hydroxychlorided species during metal sintering. Knowledge on the exact chemical nature of these species and on their formation mechanism, especially under industrial conditions, is still lacking. It is therefore of both fundamental and practical interest to undertake *in situ* studies using modern spectroscopy to identify the surface species responsible for sintering.

Extended X-ray absorption fine structure (EXAFS) spectroscopy is a powerful tool to characterize metallic supported catalysts, being especially useful for determining the local environment around metal atoms and the evolution of the local structure of chemical species formed during a dynamic process. In a previous paper (4), we investigated the sintering of unchlorinated Pt/Al_2O_3 catalysts in oxygen-containing atmospheres using EXAFS spectroscopy. We observed the existence of Pt–Pt metal distances after the oxidizing treatments and proposed that the oxidation of Pt particles only involves the outermost metal shells in a distorted PtO_2 arrangement. Recently, in an *in situ* EXAFS study (5), we investigated the redispersion of sintered Pt/Al_2O_3 catalysts, at 500°C and under $HCl/H_2O/O_2/N_2$ atmospheres, and found that $[Pt(OH)_4Cl_2]^{2-}$ species, which are formed by the attack of surface chlorided species on partially oxidized Pt particles, are responsible for Pt redispersion. The EXAFS analysis indicated that, at the end of the redispersion process, small rafts of Pt containing Cl and O in an octahedral environment and Pt particles consisting of a metallic core coated by $[Pt(OH)_4Cl_2]^{2-}$ species coexist. In this paper, we use *in situ* EXAFS spectroscopy to investigate the sintering kinetics of a fresh chlorinated Pt/Al_2O_3 catalyst in a 2% O_2/N_2 gaseous mixture. The aim was to identify the chemical nature of surface intermediate species formed during the metal sintering process.

[1] To whom correspondence should be addressed. Fax: +(54)-42-(531068). E-mail: aborgna@fiqus.unl.edu.ar.

[2] Present address: IPCMS-GSI, UMR 1046 du CNRS, Bat. 69, 23, rue du Loess, 67037, Strasbourg, France.

0021-9517/99 $30.00

2. EXPERIMENTAL

2.1. Catalyst Preparation

A catalyst containing 0.62% Pt and 0.88% Cl (catalyst A) was prepared as previously described (6). A high-purity γ-Al_2O_3 powder (Cyanamid Ketjen CK-300) was impregnated at 30°C with an aqueous solution containing H_2PtCl_6 and HCl. After impregnation, the sample was dried for 12 h at 120°C and heated in an air stream to 500°C. Then, the chlorine content was regulated using a gaseous mixture of HCl, water, and air. Finally, the sample was purged with N_2 and reduced in flowing H_2 for 8 h at 500°C. In order to prepare an unchlorinated catalyst (catalyst B), a portion of catalyst A was treated with a solution of NH_4OH (1 N) at 50°C and then washed with distilled water. After drying at 120°C, the sample was calcined in air and reduced in H_2 at 500°C. It was checked by chemical analysis that chlorine was completely removed from the sample by such ammonia treatment.

2.2. Hydrogen Chemisorption

Accessible platinum fractions were determined by hydrogen chemisorption. Prior to Pt dispersion measurements, the samples were reduced under flowing hydrogen for 2 h at 500°C and then evacuated at the same temperature. The double isotherm method was used (7): the first isotherm gave the total gas uptake and the second, obtained after 1 h of evacuation at room temperature, the weakly adsorbed gas. By the difference, the amount of strongly adsorbed H_2, $(HC)_i$, was determined. A stoichiometric ratio of $(HC)_i/Pt_S = 1$, where Pt_S implies a Pt atom on the surface, was used. The volumetric adsorption experiments were performed in a conventional glass vacuum apparatus equipped with an MKS Baratron pressure gauge. The pressure range of isotherms was 0–50 Torr, and extrapolation to zero pressure was used as a measure of the gas uptake on the metal.

2.3. TPR Measurements

The thermoprogrammed reduction (TPR) experiments were performed as described in (8), using a 5% H_2/Ar gaseous mixture at 20 cm^3/min. Prior to TPR experiments, samples were treated *in situ* in a 2% O_2/N_2 mixture at different temperatures for 30 min. Samples were heated at 5°C/min within the temperature range 25–600°C. Gases were carefully purified to remove water and oxygen traces. The water formed during reduction of the samples was eliminated by passing the gases exiting from the reactor through a cold trap before they entered the thermal conductivity cell.

2.4. EXAFS Spectroscopy

EXAFS experiments were carried out by using the synchrotron radiation emitted by the DCI storage ring at LURE. All the measurements were performed on the XAFS3 station in transmission mode by using a Si(111) double-crystal monochromator and two ion chambers filled with pure argon at atmospheric pressure. Raw data were recorded by using a special *in situ* cell equipped with aluminum windows (9), which allows work from room temperature up to 600°C in flowing controlled atmospheres. All the spectra were recorded in fast acquisition mode with an acquisition time of about 3 min for the complete spectrum (1000 eV). The energy range was about 850 eV above the Pt-L_{III} edge (11564 eV). Several spectra (4 to 10) were added before a complete analysis.

The EXAFS signal was extracted from raw data by a conventional procedure (10). A linear background was determined from the lower energy part of the spectrum below the edge and then extrapolated to higher energies. The atomic-like absorption coefficient calculated by a polynomial fit was used as spectrum normalization. The k^1 and k^3 weighted EXAFS functions were Fourier transformed (FT) over a 3–10.5 $Å^{-1}$ Kaiser window ($\tau = 9$). Then, a Fourier filtering was applied to produce the $k^3\chi(k)$ functions corresponding to the first coordination sphere, which were modeled by using an optimization program which computes coordination numbers (n), bond lengths (R), and variations of the Debye–Waller-like factors ($\Delta\sigma^2$). Finally, a reliability factor, Q, is obtained which allows the comparison of various fits (11, 12). To take into account the possibility that three different back-scatterer atoms, Pt, Cl, and O, could exist around Pt, the range in R selected to perform the inverse FT was 1–3.5 Å. During the fitting process the k range was limited between 3 and 10.5 $Å^{-1}$ ($\Delta k = 7.5$ $Å^{-1}$), and thereby the maximum number of adjustable parameters given by the Shannon criterion (13) was 12. The fitting procedure was performed on both k^1 and k^3 weighted EXAFS functions. The calculated EXAFS parameters did not differ significantly whatever the weight functions, k^1 and k^3, used.

3. RESULTS

3.1. TPR Characterization

The TPR profiles obtained after heating catalyst A in a 2% O_2/N_2 mixture for 30 min at 300, 400, 500, and 530°C are shown in Fig. 1. From inspection of Fig. 1, the presence of three reduction peaks in the TPR curves is inferred. A low-temperature peak, corresponding to the reduction of PtO_2 species, appears at ca. 100°C (4). The middle-temperature peak, which presents a maximum at about 230°C, arises from the reduction of oxy- or hydroxychlorinated Pt species (3, 5). Finally, and on the basis of previous work (14, 15), we attribute the H_2 consumption peak at ca. 360°C to a strong H_2 chemisorption at high temperature on metallic Pt. Thus, only the low- and middle-temperature peaks are related to the reduction of oxidized Pt species.

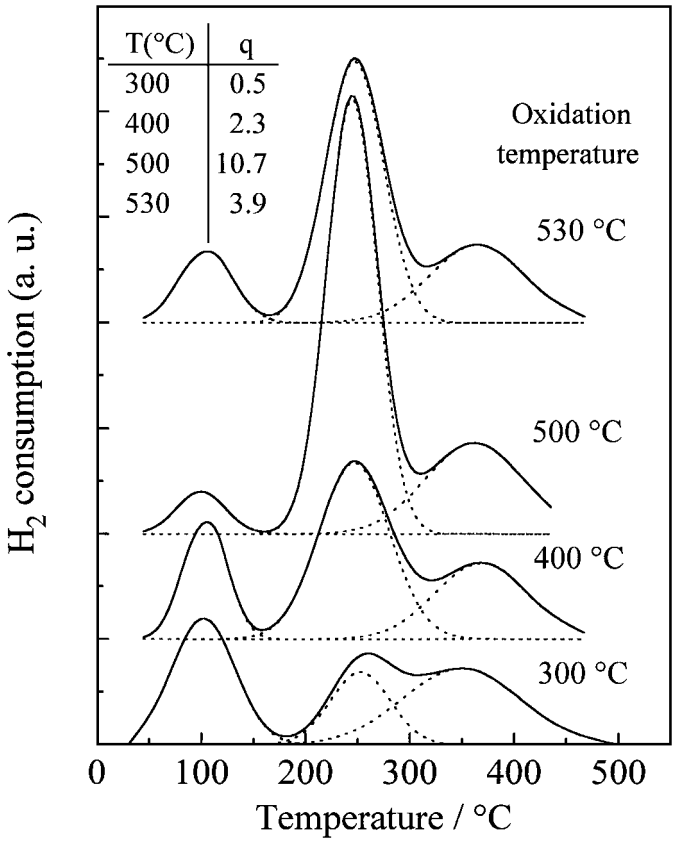

FIG. 1. TPR profiles of catalyst A following consecutive oxidizing treatments in a 2% O_2/N_2 mixture at increasing temperatures. The values of parameter q measured at each oxidation temperature are also included (see the text for definition of parameter q).

To obtain a quantitative comparison between the reduction peaks at 100 and 230°C we decomposed the TPR profiles in three reduction bands (Fig. 1) and measured by integration the relative contribution of each individual reduction peak. The obtained values of ratio q [$q = (\text{peak area})_{230^\circ C}/(\text{peak area})_{100^\circ C}$] are shown in Fig. 1 as a function of the calcination temperature. It is observed that q increases with increasing oxidation temperature from 0.5 (300°C) to 10.7 (500°C), thereby suggesting that the relative concentration of hydroxychlorinated Pt species progressively increases by heating the sample up to 500°C. Further increase in the oxidation temperature causes a steep drop in ratio q values. Thus, after heating at 530°C the value of q diminished to 3.9.

3.2. Sintering of Catalyst A: H_2 Chemisorption Results

Catalyst A was sintered in a 2% O_2/N_2 mixture at different temperatures, from 510 up to 575°C. The evolution of the relative metallic Pt dispersion, D_r, as a function of time is shown in Fig. 2. The relative Pt dispersion is defined as $D_r = D_t/D_0$, where D_0 and D_t are the values of metallic dispersions measured by H_2 chemisorption at zero time and time t, respectively. The curves representing the D_r decay as a function of time reached pseudo-steady-state values different from zero. For temperatures higher than 530°C, the Pt dispersion rapidly decreased, reaching asymptotic values after about 5 h (sintering at 575°C) and 10 h (sintering at 550°C) of sintering treatment. Sintering kinetics at 530 and 510°C were significantly slower and, as a consequence, D_r steady-state values were obtained only after about 15 and 20 h on stream, respectively.

3.3. EXAFS Results

3.3.1. Characterization of reduced catalysts A and B. Catalysts A and B, both previously reduced in pure H_2 at 300°C, were characterized by EXAFS spectroscopy. To determine the Pt–Pt, Pt–O, and Pt–Cl distances in the first coordination sphere, we used the phase shifts and backscattering amplitudes extracted from reference compounds. Table 1 gives the mean coordination numbers around platinum (n) and the distances between platinum and backscattering atoms (R) in the reference compounds (Pt foil, PtO_2, and K_2PtCl_6), calculated from crystallographic data available in the literature (see references in Table 1). In the case of platinum oxide we considered a mean Pt–O

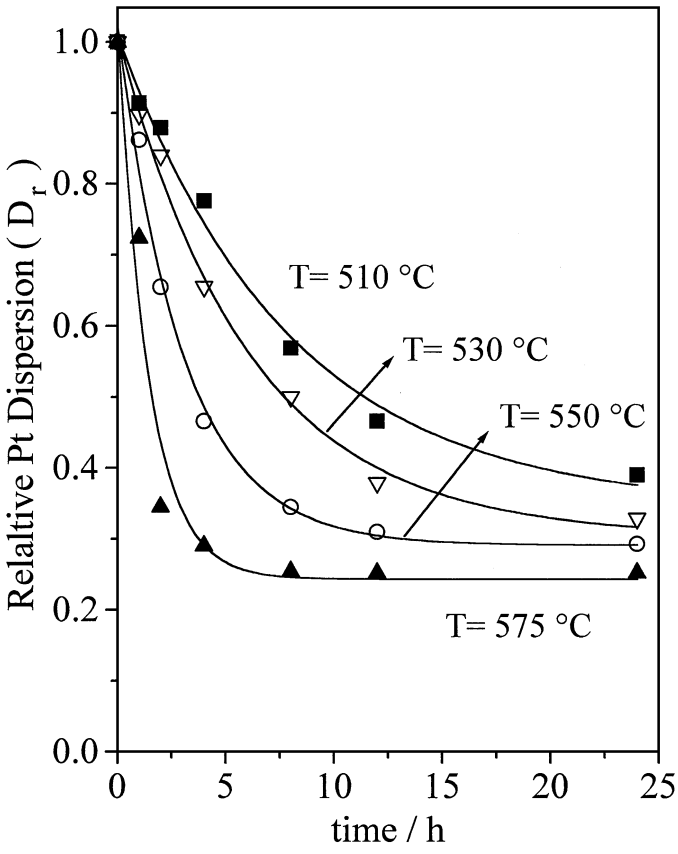

FIG. 2. Relative Pt dispersion (D_r) vs time curves. Sintering treatments in a 2% O_2/N_2 mixture at different temperatures.

TABLE 1

Structural Data of the Reference Compounds

Compound	Back-scatterer	n	R (Å)	Ref.
Pt foil (4 μm thick)	Pt	12	2.772	(25)
PtO_2	O	2 + 4	1.984, 2.004	(26)
K_2PtCl_6	Cl	6	2.341	(27)

distance of 1.987 Å for the extraction of phase-shift and back-scattering amplitude. Figure 3 shows the FTs of reference compounds. Peak (a) corresponds to the first coordination sphere in bulk metal whereas peak (b) is attributed to the first Pt–Pt distances in PtO_2.

The FT plots and the EXAFS parameters obtained on reduced catalysts A and B are presented in Fig. 4 and Table 2, respectively. Table 2 shows that the values of n, R, and $\Delta\sigma^2$ determined on catalyst A were similar to those calculated on catalyst B, thereby suggesting that reduction of Pt/Al_2O_3 catalysts in pure H_2 at 300°C leads to the same type of metal phase, irrespective of the chlorine content on the support. The parameter values given in Table 2 for reduced catalyst A ($R = 2.75$ Å, $n = 7.6$, $\Delta\sigma^2 = 0.0036$) are taken as the initial values in the sintering treatment of this catalyst, just before introduction of the 2% O_2/N_2 mixture at 300°C.

3.3.2. In situ sintering of catalyst A. To obtain insight on the sintering mechanism, an *in situ* EXAFS study in fast acquisition mode was carried out. Because a rather slow sintering rate is required to monitor catalyst changes by EXAFS spectroscopy, and taking into account the results in Fig. 2, we selected a temperature of 525°C for performing the *in situ* sintering of catalyst A. The EXAFS results are presented in Table 3 and Figs. 5 to 7. Due to the difficulty of performing EXAFS analysis at high tempreature, the coordination values reported in Table 3 must be taken with care. The errors are estimated to 15–20%, especially for Pt–O and Pt–Cl coordinations. The first spectrum reported in Table 3, spectrum at zero time, corresponds to the spectrum registered just before the sintering treatment under oxidizing mixture was started. To define the nature of the chemical species formed in the sintering process, we first attempted to detect the presence of chlorine in the immediate Pt surroundings. In Fig. 5 we compare the experimental results with the predictions of modeling the Pt first coordination sphere in the absence (Fig. 5a) or in the presence (Fig. 5b) of chlorine in the immediate surroundings of platinum, after 50 min of sintering treatment. The differences in the quality of the fits, as well as the Q values, clearly suggest that a good fit is only obtained by modeling the Pt first coordination sphere in the presence of chlorine. The same conclusion was reached by modeling the EXAFS results obtained at different periods of time-on-stream.

The FTs obtained on catalyst A for several sintering times, from 0 up to 360 min, are shown in Fig. 6 and illustrate the evolution of the radial distribution around platinum in this initial period. The 2% O_2/N_2 mixture was introduced over reduced catalyst A at 300°C, after it was flushed with

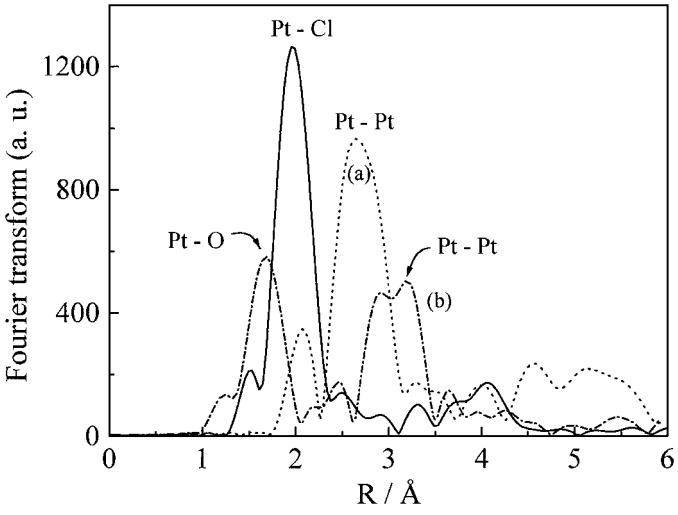

FIG. 3. Fourier transforms of model compounds used as references for the EXAFS analysis: Pt foil (dotted line); PtO_2 (dashed line); K_2PtCl_6 (full line).

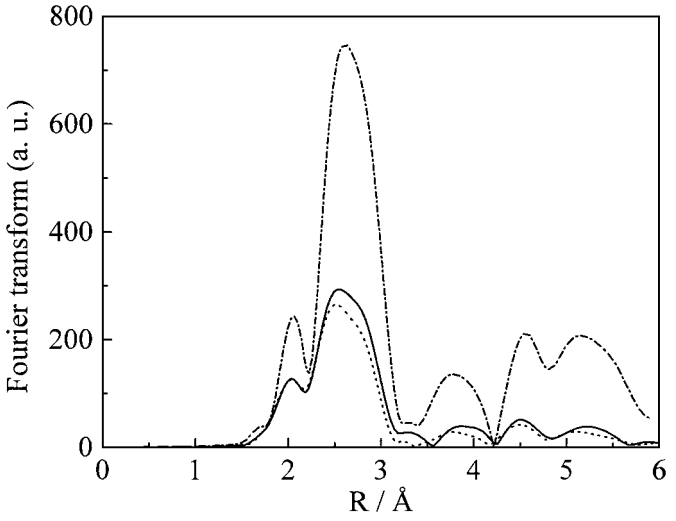

FIG. 4. Fourier transforms of reduced catalysts A (full line) and B (dotted line) compared with that of Pt foil (dashed line).

TABLE 2

EXAFS Parameters for Reduced Pt/Al_2O_3 Catalysts

Catalyst	n	R (Å)	$\Delta\sigma^2$
Catalyst A	7.6	2.75	0.0036
Catalyst B	7.4	2.76	0.0025

TABLE 3

Parameters Deduced from EXAFS Analysis during the Sintering Process

		Pt–O			Pt–Cl			Pt–Pt			
Time (min)	T (°C)	n	R	$\Delta\sigma^2$	n	R	$\Delta\sigma^2$	n	R	$\Delta\sigma^2$	Q (%)
0	300	—	—	—	—	—	—	7.6	2.75	0.0036	6.03
5	413	2.2	2.04	0.0198	0.8	2.50	0.0151	4.9	2.73	0.0149	9.81
15	474	3.3	1.99	0.0289	1.9	2.46	0.0149	5.9	2.70	0.0906	6.27
30	498	4.4	2.01	0.0436	2.0	2.59	0.0146	4.7	2.73	0.0827	3.34
50	510	3.4	1.98	0.0366	1.2	2.55	0.0148	4.0	2.67	0.0853	7.88
90	—	3.9	1.99	0.0390	0.8	2.69	0.0153	2.4	2.68	0.0865	7.27
120	—	3.5	1.99	0.0387	0.5	2.80	0.0182	3.2	2.70	0.0742	7.00
150	523	3.9	2.01	0.0351	0.4	2.77	0.0150	2.9	2.69	0.0847	6.33
180	—	3.5	2.01	0.0389	0.3	2.72	0.0145	3.9	2.71	0.0854	3.15
220	524	3.8	2.00	0.0440	0.2	2.74	0.0255	3.3	2.71	0.0723	11.40
360	527	3.6	2.01	0.0450	0.7	2.68	0.0380	3.0	2.69	0.0649	9.48
420	—	3.5	1.98	0.0390	0.7	2.59	0.0387	4.1	2.70	0.0629	14.64
480	—	3.2	1.99	0.0363	0.7	2.62	0.0439	4.5	2.70	0.0634	6.98
540	—	4	2.03	0.0420	0.7	2.55	00450	3.8	2.68	0.0663	7.64
600	528	3.1	1.98	0.0451	0.4	2.67	0.0394	4.2	2.69	0.0639	11.02
720	—	3.6	2.00	0.0409	0.5	2.66	0.0417	4.7	2.72	0.0672	3.34

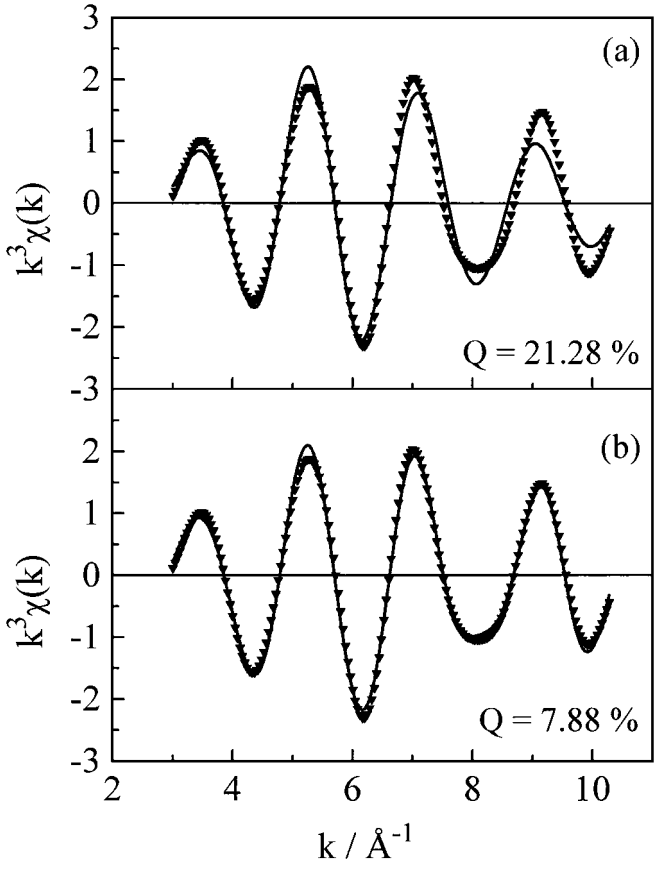

FIG. 5. Experimental (triangles) and modeled (full line) EXAFS contributions around Pt atoms after 50 min of sintering treatment: (a) fit without Cl, (b) fit with Cl atoms introduced in the first coordination shell of Pt.

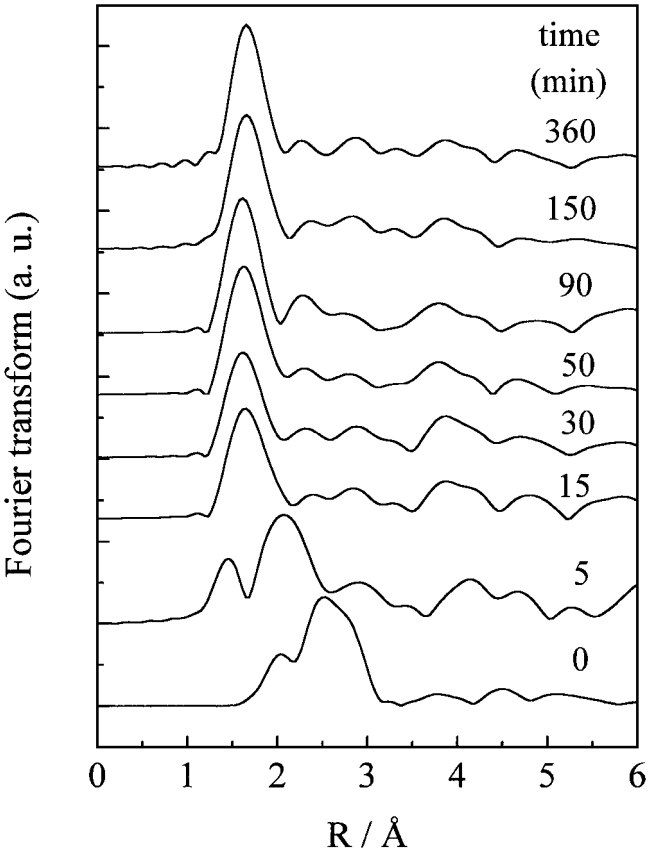

FIG. 6. Evolution of radial distribution functions around platinum as a function of time.

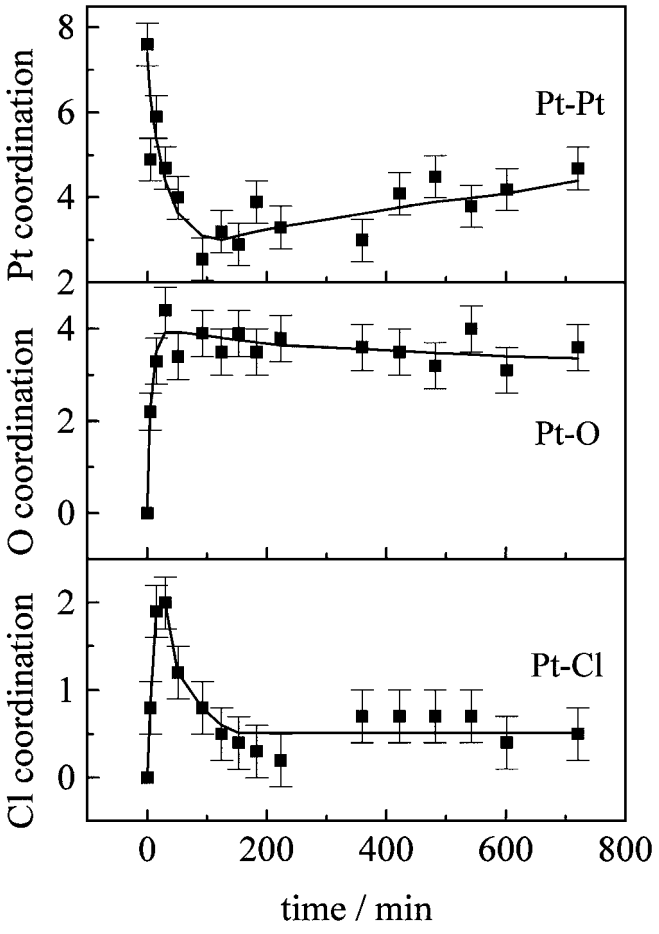

FIG. 7. Evolution of Pt, Cl, and O coordinations around platinum as a function of time.

dried helium. The temperature was then rapidly raised from 300 up to 510°C in 50 min and finally slowly stabilized at about 525–528°C. The platinum surroundings in reduced catalyst A were deeply modified by the oxidizing treatment at increasing temperatures. Once the catalyst reached the stabilization temperature, after about 80 min, the surroundings of platinum appeared qualitatively stabilized and did not undergo further significant modifications during the run.

In Table 3 and Fig. 7 we present the evolution of the EXAFS parameters and of the coordination numbers in Pt, O, and Cl as a function of time. The variation of adjustable parameter ΔE_0 (not reported here) was within 5 eV around the values taken for the reference compounds. The precision of the coordination numbers is about 15–20%, as illustrated by the error bars in Fig. 7. At the beginning of the sintering treatment, the system is in constant evolution due to the increase of temperature and the formation of partially oxidized Pt particles. These facts could produce a large imprecision on both coordination number and disorder factor (Debye–Waller factor). Moreover, the effect of the system evolution may be emphasized by the summation of 4–5 successive spectra. Hence the EXAFS parameters determined during the first 50 min could be overestimated and must be taken with care. From the data in Table 3 and Fig. 7 we can distinguish three successive steps during the oxidation and sintering of catalyst A. In the initial step, from 300 to 500°C, the Pt–Pt coordination largely decreases from 7.4 to 4.7 while the Pt–Cl and Pt–O coordinations increase from 0 to 2 and from 0 to about 4, respectively. At the end of this first step of ca. 30 min the $n_{\mathrm{Pt-O}}/n_{\mathrm{Pt-Cl}}$ ratio is nearly 2. The second step ranges from 30 min up to about 120 min, and is characterized by a clear diminution in the Pt–Cl coordination, from 2 to about 0.5. The Pt–Pt coordination monotonically decreases, reaching a value of about 3 after 120 min on stream. In the final step, from 120 min up to the end of the run, the temperature is stabilized (525–528°C). The Pt–Cl coordination remains nearly constant (0.5) whereas the Pt–O coordination slightly decreases and the Pt–Pt coordination monotonically increases.

During the sintering treatment, the Pt–O and Pt–Pt distances measured on catalyst A do not largely differ from those of reference compounds. The Pt–O distance appears very stable at 2.0 Å, close to that observed in PtO_2. The mean value for the Pt–Pt distance is about 2.71 Å, which is slightly shorter than that calculated in Pt foil (2.77 Å). In contrast to the Pt–Pt and Pt–O distances, the Pt–Cl distance during the sintering treatment significantly differs from that in K_2PtCl_6 (2.34 Å), varying between 2.46 and 2.80 Å.

4. DISCUSSION

A main observation of this study is that chlorine was present in the first shell around platinum during the entire sintering process. As is shown in Fig. 5, the experimental data were well fitted only by including chlorine in the first coordination sphere of platinum. Since the oxidizing mixture used here did not contain chlorided compounds, this result indicates that chlorine originating from the support was always in the immediate surroundings of Pt during the metal sintering.

The EXAFS results allowed us to distinguish three consecutive steps during the oxidizing treatment of catalyst A. In the first step, from 300 to 500°C, the continuous increase in Pt–O and Pt–Cl coordinations suggests the progressive formation of hydroxychlorided complexes such as $[Pt_s(OH)_xCl_{(6-x)}]^{2-}$. Consistently, the Pt–Pt coordination decreases from 7.6 in the reduced catalyst to 4.7 at the end of this first step. When the temperature reached 500°C the $n_{\mathrm{Pt-O}}/n_{\mathrm{Pt-Cl}}$ ratio was 2. Such a $n_{\mathrm{Pt-O}}/n_{\mathrm{Pt-Cl}}$ ratio corresponds to a value of $x = 2$ and strongly suggests the formation of $[Pt(OH)_4Cl_2]^{2-}$, which is a more stable species in the series of $[Pt_s(OH)_xCl_{(6-x)}]^{2-}$ complexes (16, 17). Formation of $[Pt(OH)_4Cl_2]^{2-}$ is consistent with previous studies on redispersion of Pt/Al_2O_3 catalysts which showed that

$[Pt(OH)_4Cl_2]^{2-}$ was the exclusive species formed during the redispersion process under oxychlorinated atmospheres (5). The progressive formation of hydroxychlorinated species with increasing temperature is also revealed by the TPR results. Figure 2 shows that the sequential heating of catalyst A at 300, 400, and 500°C in 2% O_2/N_2 atmospheres increased the TPR peak at 230°C resulting from reduction of hydroxychlorinated Pt species at the expense of the low-temperature peak which corresponds to Pt oxide species.

In the second step, the temperature was slowly raised from 500 up to 525°C. This 90-min period was characterized by a significant decrease in Pt–Cl coordination, from 2 to about 0.5, together with an enlargement of the Pt–Cl distance. A probable explanation for these EXAFS results, which show the modification of the Pt–Cl bonding for temperatures higher than 500°C, is that the gradual heating from 500 to 525°C partially removes chlorine from the catalyst and thereby diminishes the concentration of chlorine on the alumina support. This assumption is supported by the TPR results. Figure 2 shows, in fact, that upon the catalyst treatment at 530°C the reduction peak at 230°C decreases and that at 100°C increases, as compared with the corresponding peaks in the TPR profile of the sample oxidized at 500°C. This is consistent with a retransformation of $[Pt(OH)_4Cl_2]^{2-}$ into oxidized Pt species caused by a diminution in the Cl concentration on the support. On the other hand, low values of the Debye–Waller-like factor associated with the Pt–O bond were observed during this second step (Table 3). This strongly suggests that even at temperatures as high as 500–525°C the oxygen octahedron around a platinum atom is stable and rather well ordered. If ordered PtO_2 around the platinum core exists, the Pt–Pt distance would be the average of distances in metal Pt and in bulk PtO_2 (3.15–3.18 Å), and, as a consequence, the Pt–Pt distance computed by EXAFS would be larger than 2.77 Å. Therefore, since the Pt–Pt distance determined by EXAFS (2.71 Å) is much lower than in bulk metal, we could reject the occurrence of ordered PtO_2 around the platinum core. The absence of a long-range order allows the location of residual chlorine species either between the PtO_6 octahedra or at the Pt-oxidized surface shell. In this period, the Pt–Cl distance increased from 2.55 to 2.80 Å. These large R_{Pt-Cl} values suggest that the chlorine atoms were more weakly bonded to platinum in catalyst A as compared to a stoichiometric compound such as K_2PtCl_6 ($R_{Pt-Cl} = 2.341$ Å, Table 1). A progressive formation of disordered nonstoichiometric oxychlorinated species at the expense of stoichiometric $[Pt(OH)_4Cl_2]^{2-}$ complexes may explain the Pt–Cl distance enlargement observed in this period.

In the final step, performed at 525–528°C, the Pt–Pt coordination monotonically increases with time-on-stream while the n_{Pt-O} value slightly decreases. The Pt–Cl coordination remains essentially constant ($n_{Pt-Cl} \cong 0.5$). In parallel *ex situ* experiences we followed the evolution of the Pt dispersion as a function of time and observed that treatment of catalyst A at 510 or 530°C in a 2% O_2/N_2 mixture strongly sinters the metallic component (Fig. 2). Similarly, the n_{Pt-Pt} increase observed in this third step presumably reflects a progressive increase in the mean Pt crystallite size. To obtain insight on the Pt chemical species involved during this Pt particle growth process, we attempted to model our EXAFS results based in the evolution of the mean Pt particle size with time (sintering curve at 530°C in Fig. 2). The modeling of the results was performed by assuming that, at a given sintering time, all the partially oxidized Pt particles have the same size and shape (cubo-octahedra or truncated octahedra); we also assumed that the particle shape is not significantly changed by the reduction treatment needed for measuring the mean Pt particle size by H_2 chemisorption in Fig. 2. Relying on a previous work (4), we assumed that in the sintering process the oxidized Pt particles are covered by a coating of oxychlorinated species. The coat thickness should be consistent with both the mean Pt particle size deduced from the sintering curve in Fig. 2 and the Pt–Pt coordination number extracted from *in situ* EXAFS experiments (Table 3). Formation of this oxychlorinated coat is equivalent to removing one or several shells of platinum from the Pt particle surface. In Fig. 8 we compare the experimental results with the modeling predictions obtained by considering that the Pt particles are covered by either a single or a double shell of oxychlorinated species. It is observed that, after about 4 h of treatment, the experimental n_{Pt-Pt} values are in good agreement with those determined by assuming that the Pt particles are covered by a double-coating of oxychlorinated species.

Previous work on sintering of supported metal catalysts has shown that the metal particle growth on a substrate occurs mainly by migration of crystallites (18) and single-atom diffusion (19, 20). Both these mechanisms are known to take place simultaneously (21). In the experimental conditions used in this work, the Pt migration occurs in the presence of oxygen in the gas phase and of Cl^- and OH^- groups on the support. The oxychlorinated Pt species detected by TPR and EXAFS are probably formed then by migration of oxidized Pt species over a partially hydroxylated and chlorided alumina surface. Our previous works (2, 5, 22) and the results reported in the present study suggest that the nature and the amount of oxychlorinated species formed on the oxidized Pt particle surface depend on both the sintering temperature and the chlorine concentration on the support. In Scheme 1 we give a simplified representation of the oxychlorided species that we proposed to form during oxidation (end of the first step, at 500°C) and sintering (third step, at 525°C) of catalyst A.

In the third step, the Pt–Pt metal coordination increased from 2.5 to 5 at the end of the run. On basis of the above-proposed cherry model, these n_{Pt-Pt} values imply that the metallic Pt core diameter increased from 12–15 Å to about

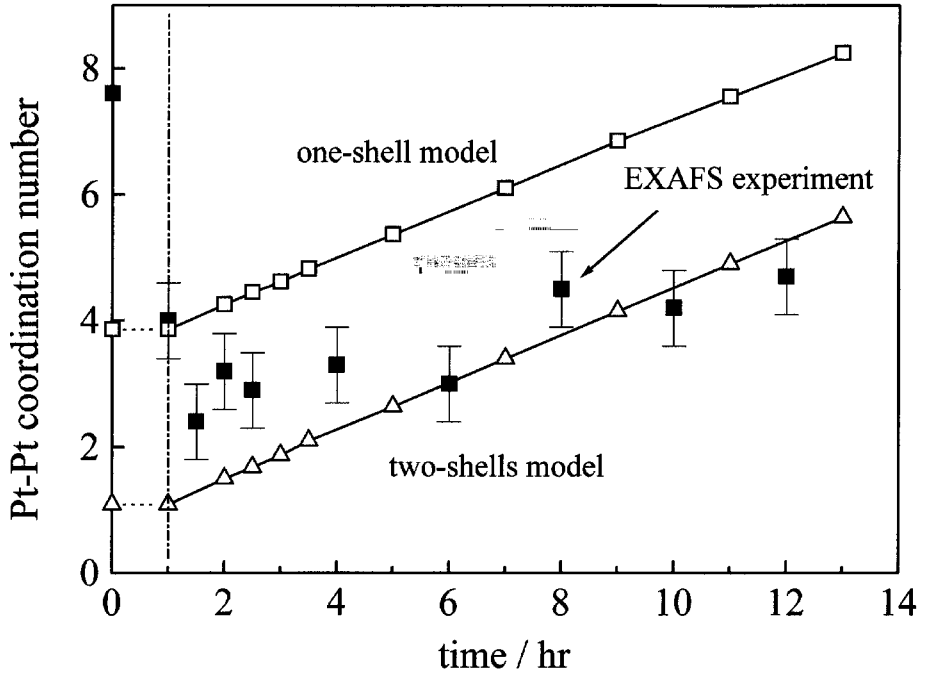

FIG. 8. Evolution of Pt–Pt coordination as a function of time: experimental EXAFS data (■); modeling of Pt particles covered by one (□) or two (△) surface shells of oxychlorided species.

30 Å. On the other hand, during this third step the Pt–Pt distance remained essentially constant ($R_{Pt-Pt} \cong 2.71$ Å) and shorter than that in the bulk metal ($R_{Pt-Pt} = 2.77$ Å). Although similar Pt–Pt distance shortenings have been reported in very small Pt particles (10, 23), i.e., lower than 15 Å, we observe here R_{Pt-Pt} contractions in Pt particles as large as 30 Å. It appears that the double-coating of oxidized platinum species induces constraints on the metallic Pt core, which results in the shortening of the Pt–Pt distance. In a earlier study, we found that during redispersion of Pt/Al_2O_3 catalysts in $HCl/H_2O/O_2/N_2$ atmospheres the mean Pt–Pt distance is about 2.80 Å (5). This large discrepancy between the R_{Pt-Pt} values determined in sintering and redispersion phenomena may be explained by the fact that during the redispersion process two kinds of Pt species are formed (5). A part of the Pt atoms forms particles consisting of a metallic Pt core covered by oxychlorinated species. The other part forms small rafts containing Cl and O in an octahedral environment. These two forms (particles and rafts) are in equilibrium. In the raft structures the Pt–Pt distance is about 3.18 Å (24), and this large R_{Pt-Pt} value explains the large mean Pt–Pt distance deduced from EXAFS experiments during redispersion.

Finally, we noted that the general behavior of a chlorinated Pt/Al_2O_3 catalyst during an oxidizing treatment appears different from that observed on an unchlorinated catalyst. In a previous work (4), we found that only a single coating of PtO_2 is formed on the metallic Pt particle when a nonchlorided Pt(0.6 wt%)/Al_2O_3 catalyst is treated in pure O_2 at 300°C. On chlorinated catalysts, the presence of chlorine on the carrier at the beginning of the oxidizing treatment is likely responsible for a more deep attack of platinum particles, causing the formation of a double coating of $[Pt(OH)_4Cl_2]^{2-}$ complexes.

These results, as well as the data presented in Ref. (5), provide some insight into the subtle frontier between the sintering and redispersion processes of platinum particles. The occurrence of chlorine and water, either adsorbing from the gas phase or diffusing onto the surface, is the key to switching towards growth (sintering) rather than depopulation (redispersion) of Pt particles. In the presence of chlorided as well as hydroxyl groups, the occurrence of Cl^-- or OH^--terminated surface inhibits the surface diffusion of the deeply oxygenated platinum particles. The equilibrium between the raft and particle morphologies determines a

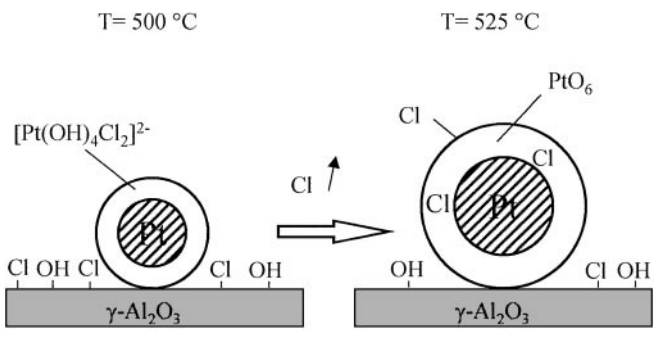

SCHEME 1

drop of the mean particle size, subsequently to the reduction of the catalyst. Otherwise, the absence of Cl^-- or OH^--terminated surface enhances the surface diffusion of the less deeply oxychlorinated particles, and coalescence does occur, determining now a sintering process. In the case of the treatment of a chlorinated catalyst by a dried and unchlorided oxidizing atmosphere, the transient chlorided surface allows first a redispersion, followed by sintering as soon as the chloride is removed.

5. CONCLUSIONS

In the sintering of Pt/Al_2O_3-Cl catalysts under dried oxygen-containing atmospheres, oxychlorided Pt species are formed by migration of oxidized Pt particles over the partially chlorided support. Initially, during the catalyst heating up to 500°C, Pt particles consisting of a metallic Pt core covered by $[Pt(OH)_4Cl_2]^{2-}$ species are formed. Increasing the temperature further to 525°C partially removes chlorine from the support, causing the progressive formation of disordered nonstoichiometric oxychlorinated species at the expense of stoichiometric $[Pt(OH)_4Cl_2]^{2-}$ complexes. Finally, during the Pt crystallite growth at 525°C, the Pt metallic core is covered by a double-coating of stable and well-ordered PtO_6 octahedra. However, no long-range order exists in the Pt-oxidized surface shell which allows the location of residual chlorine species between the PtO_6 octahedra.

ACKNOWLEDGMENTS

We are greatly indebted to the LURE staff for dedicated runs. During the X-ray absorption experiments we greatly appreciated the technical assistance of F. Villain. We are grateful to Mr. E. Benvenuto for carrying out TPR experiments. Prof. J. Barbier and Prof. J. M. Parera are thanked for their constant interest during the progress of this work, which was part of the "Programme International de Coopération Scientifique" (PICS 74) between CNRS (France) and CONICET (Argentina).

REFERENCES

1. Callender, W. L., and Miller, J. J., *in* "Proceedings, 8th International Congress on Catalysis, Berlin, 1984," Vol. 2, p. 491. Dechema, Frankfurt-am-Main, 1984.
2. Garetto, T. F., Borgna, A., Benvenuto, E., and Apesteguía, C.R., *in* "Proceedings, 12th Iberoamerican Symposium on Catalysis," Vol. 1, p. 585, 1990.
3. (a) Lieske, H., Lietz, G., Spindler, H., and Völter, J., *J. Catal.* **81**, 8 (1983). (b) Lietz, G., Lieske, H., Spindler, H., Hamke, W., and Völter, J., *J. Catal.* **81**, 17 (1983).
4. Borgna, A., Le Normand, F., Garetto, T. F., Apesteguía, C. R., and Moraweck, B., *Catal. Lett.* **13**, 175 (1992).
5. Le Normand, F., Borgna, A., Garetto, T. F., Apesteguía, C. R., and Moraweck, B., *J. Phys. Chem.* **100**, 9068 (1996).
6. Borgna, A., Garetto, T. F., Monzón, A., and Apesteguía, C., *J. Catal.* **146**, 69 (1994).
7. Sinfelt, J. R., Cartier, J. L., and Yates, D. F. C., *J. Catal.* **24**, 283 (1972).
8. Apesteguía, C. R., Garetto, T., and Borgna, A., *J. Catal.* **106**, 73 (1987).
9. Lytle, F. W., Greegor, R. B., Marques, E. B., Sandstroem, D. R., Via, G. H., and Sinfelt, J. H., *J. Catal.* **95**, 546 (1985).
10. Moraweck, B., Clugnet, G., and Renouprez, A., *Surf. Sci.* **106**, 35 (1981).
11. Schwartz, L. H., and Cohen, J. B., *in* "Diffraction from Materials," p. 295. Academic Press, New York, 1977.
12. Borgna, A., Moraweck, B., and Renouprez, A., *J. Chim. Phys.* **86**, 1719 (1989).
13. Crozier, E. D., Rehr, J. J., and Ingalls, R., *in* "X-Ray Absorption Principles, Applications, Techniques of EXAFS, SEXAFS and XANES" (D. C. Koningsberger and R. Prins, Eds.), p. 395. Wiley, New York, 1988.
14. Menon, P. G., and Froment, G. F., *J. Catal.* **59**, 138 (1979).
15. Menon, P. G., and Froment, G. F., *Appl. Catal.* **1**, 31 (1981).
16. Wells, A. F., *in* "Structural Inorganic Chemistry" (A. F. Wells, Ed.), p. 556. Clarendon, Oxford, UK, 1967.
17. Doronin, N. P., Tsymbal, T. V., and Duplyakin, V. K., *React. Kinet. Catal. Lett.* **32**, 399 (1986).
18. Ruckenstein, E., and Pulvermacher, B., *J. Catal.* **29**, 224 (1973).
19. Flynn, P. C., and Wanke, S. E., *J. Catal.* **34**, 390 (1974).
20. Wymblatt, P., and Gjostein, N. A., *Acta Metall.* **24**, 1175 (1976).
21. Ruckenstein, E., and Dadyburjor, *J. Catal.* **48**, 73 (1977).
22. Garetto, T. F., Borgna, A., and Monzón, A., *J. Chem. Soc. Faraday Trans.* **92**(14), 2637 (1996).
23. Guyot-Sionnest, N., Villain, F., Bazin, D., Dexpert, H., Le Peltier, F., Lynch, J., and Bournonville, J. P., *Catal. Lett.* **8**, 283 (1991).
24. Lagarde, P., Murata, T., Vlaic, G., Dexpert, H., Freund, E., and Bournonville, J. P., *J. Catal.* **84**, 333 (1983).
25. Schröder, R. H., Schmitz-Pranghe, N., and Kohlhaas, R., *Zeitsch. Metallkunde* **63**, 12 (1972).
26. Range, R. J., Rau, F., Klement, U., and Heynes, A. M., *Mater. Res. Bull.* **22**, 1541 (1987).
27. Busch, R. H., Galloni, E. E., and Haitz, C. R., *Anal. Asoc. Quim. Argentina* **39**, 55 (1951).